

# MATHEMATICAL MODELS THROW LIGHT ON GALVANIZING LINES <sup>1</sup>

*Diego Migliorino<sup>2</sup>  
Gabriel Cervellini<sup>3</sup>  
Javier I. Etcheverry<sup>4</sup>  
Alejandro Jacobsen<sup>5</sup>*

## **Abstract**

We summarize in this presentation the achievements of several years of modeling efforts at SIDERAR's hot dip galvanizing lines. We discuss developments for different concrete applications: a mathematical model of the non-oxidizing furnace, an energy balance of the Zn pot, and a study of the factors that interfere with the accurate strip temperature measurement with the lines infrared pyrometers.

**Key words:** Hot dip Galvanizing lines; Continuous annealing; Oxycombustion; Infrared pyrometers; Zn pot; Mathematical models.

---

<sup>1</sup> 43° Seminário de Laminação- Processos e Produtos Laminados e Revestidos- 17 a 20 de outubro de 2006- Curitiba- PR- Brasil

<sup>2</sup> Hot-Dip Process Engineer, Ternium Siderar

<sup>3</sup> Hot Dip Process Engineer, Ternium Siderar

<sup>4</sup> Center for Industrial Research, Tenaris Siderca

<sup>5</sup> Coating Production Manager, Ternium Siderar

## INTRODUCTION

In this paper we summarize the achievements of several years of modeling efforts at SIDERAR's hot dip continuous galvanizing lines. We discuss developments for different specific applications: a mathematical model of the non-oxidizing furnace (NOF), a study of the factors that interfere with the accurate strip temperature measurement inside the furnaces, and an energy balance of the Zn pot.

SIDERAR's HDG lines have the typical design of the EFCO horizontal furnace represented in Figure 1. As the strip enters the furnace, it is heated in the tunnel by the flue gases coming from the direct fire furnace (DFF). Inside the latter, it receives almost all of the required energy (to reach recrystallization temperature in the case of cold rolled material, for instance). Up to this point the strip is in direct contact with combustion gases. In the rest of the process the strip is heated a bit further in the radiant tube furnace (RTF), and then cooled down to about the molten Zn bath temperature in the Jet-Coolers section, all of this in a controlled reducing atmosphere.

The main strip temperature checkpoints are located at the exit of the direct fire furnace (vestibule pyrometer), at the exit of the radiant tube furnace, and at the turn roll hood (TRH). The first one enables to control the temperature at the exit of the main heating stage, while the second gives information on the maximum strip temperature achieved during the thermal cycle, and the third provides an indication of the temperature at which the strip enters the Zn bath.

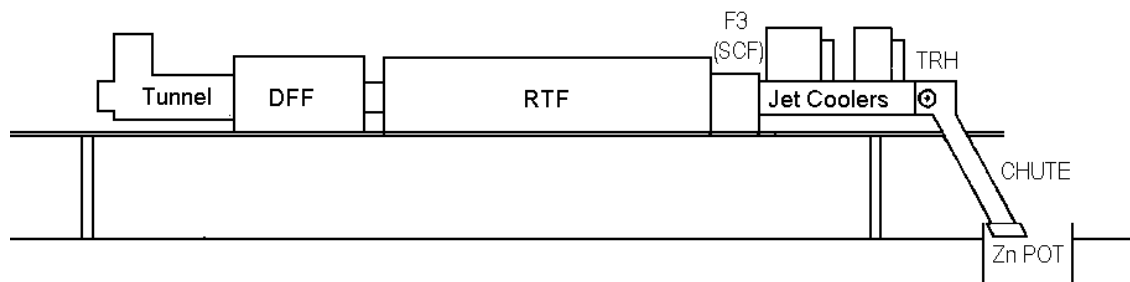


Figure 1. Typical horizontal hot dip continuous galvanizing line.

## DIRECT FIRE FURNACE MODELING

As the DFF is the main heating stage, and was a productivity limiting factor for products over 0.56 mm in SIDERAR's CGL#1 line, a large effort was devoted to develop a model of the DFF that could be used to analyze our two HDG lines and study both transient and stationary conditions. As it has been described elsewhere, we will only briefly present the model structure, and we will instead concentrate in some of the issues that have been analyzed using this tool.<sup>(1,2)</sup>

### Mathematical Model

The mathematical model of the DFF was developed on the basis of a "long-furnace" assumption, as a trade-off between precision and simplicity.<sup>(3)</sup> As radiation is the major means of heat exchange in this kind of high temperature furnace, radiation from the combustion gases must be dealt with care. To this end, we used a proven wide band model to describe the emission of CO<sub>2</sub> and water vapor.<sup>(1,4)</sup>

The length of the furnace was divided in an appropriate number of slices (typically between 20 and 40). Each slice is described by the corresponding wall surface, gas, and strip temperatures, and by the inner wall temperature as a function of the penetration inside the wall. Given these temperatures, consideration of the radiative equilibrium inside the slice allows to compute the net radiative fluxes entering the strip and the wall (Figure 2). Adding an estimation of the convective exchanges, the total fluxes are obtained. In turn, these are used to update the temperatures, by using the energy conservation for the strip and the gases, and the heat equation to describe the temperature evolution inside the wall. The temperature dependence of both strip and refractory specific heats and thermal conductivities are taken into account. This is particularly important in the case of the strip, because at temperatures close to 700 °C the specific heat presents a strong peak corresponding to the ferromagnetic transition.<sup>(5)</sup>

This procedure is applied for each time step, in order to compute the temperatures of the wall surface, gases, and strip as a function of both the coordinate along the furnace and the time, and the evolution of the temperature inside the furnace wall. The input variables are the strip dimension (thickness and width), the line speed, and the gas flow-rate in each of the zones in which the furnace is divided. The reading of the thermocouples placed inside the furnace is also computed, based on the assumption that they are always in equilibrium with the incoming energy fluxes (i.e. the net flux through their surface is zero).

The model can also be used to provide stationary predictions, both by waiting for the system to reach an equilibrium situation holding the input parameters constant, or by solving the nonlinear system of equations corresponding to steady state. In order to increase its usefulness, the model was coupled with optimization routines that allow to compute maximum line speeds compatible with given strip gauge and temperature at the exit of the DFF, gas consumption by furnace zone that give prescribed zone temperatures, etc, eventually adding suitable constraints. For instance, when computing the maximum line speed for a given product, the solutions leading to unacceptably high wall temperatures should not be taken into account.

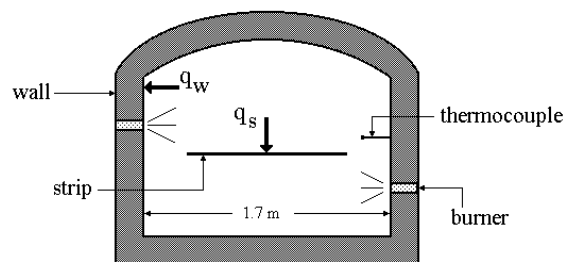


**Figure 2.** Schematic transverse section of the DFF. Here  $q_w$  and  $q_s$  denote the net energy fluxes to the wall and the strip, respectively.

### Maximum Productivity

One of the first uses of the stationary model was to compute the maximum predicted productivity for each line and strip dimension, based on the maximum allowed furnace zone temperatures, the maximum zone gas flowrate and the desired strip temperature at the exit of the DFF. This analysis permitted to identify a few products in one of the lines that were not processed at the optimum speed. Still more important, it reduced the trial period required to find the right processing conditions for new materials, particularly when for metallurgical reasons some special strip

temperatures had to be achieved. As an example, Figure 3 shows the maximum productivity predicted in ton/h for SIDERAR's CGL #2, assuming a maximum DFF zone temperature of 1250 °C, a target temperature of 630 °C at the exit of the DFF, and a maximum line speed of 115 m/min.

### Limiting Factors

Of more conceptual interest was the precise identification of the DFF limitations at play for each HDG line and product. The main limitations are introduced by the maximum line speed, the maximum furnace zone temperature, and the maximum gas flow rate. The first one normally affects light gauges, that can be easily heated. The second and third ones are important for thicker products, depending on the strip width: thick and wide strips tend to be limited by the furnace firepower, because of the high mass flow through the furnace, while thick and narrow strips are normally limited by the maximum zone temperature (see Figures 3 and 4). This is due to the fact that in high-temperature furnaces heating is achieved mostly by radiation, and the maximum radiative flux is limited by the maximum achievable furnace temperature. Figure 4 exhibits a schematic diagram of the limiting factors obtained for SIDERAR's CGL #2 under the same conditions of Figure 3.

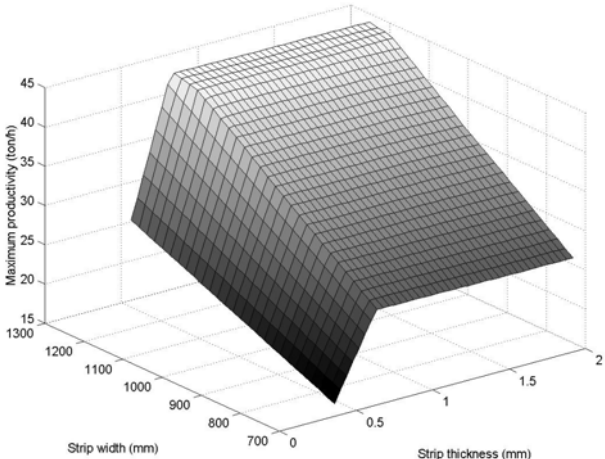


**Figure 3.** Maximum productivity as a function of strip width and thickness, for the SIDERAR's CGL #2 furnace, assuming a maximum line speed of 115 m/min, maximum wall temperature of 1250 °C, and a strip temperature at the exit of the DFF of 630 °C.

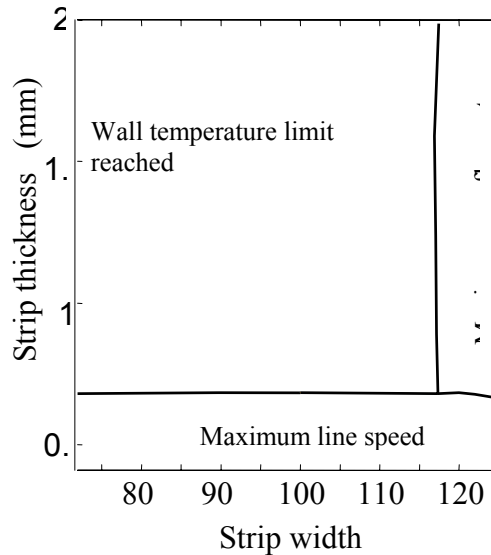


**Figure 4.** Diagram of the limiting factors for DFF productivity, for SIDERAR's CGL #2, assuming a maximum line speed of 115 m/min, maximum wall temperature of 1250 °C, and a strip temperature at the exit of the DFF of 630 °C.

### Natural Gas/Oxygen Burners Addition in HDG#1

From the analysis of the previous section it followed that one of SIDERAR's lines was limited by the heating capacity for a significant range of products. Several alternatives were considered in order to alleviate this situation, and the installation of natural gas/oxygen burners in the tunnel (Figure 1) emerged as a simple and promising technique<sup>6,7</sup>. The simplicity was related to the fact that only minor modifications to the tunnel were required to incorporate four burners of 300 kW each, which represented a 17 % increase in the fire power of the furnace. As the addition was to be performed in the tunnel, that was already hot due to the flue gases from the furnace flowing at a high speed, little gain was expected with conventional air-gas burners. As the oxycombustion flame temperature is higher because no N<sub>2</sub> has to be heated up to flame temperature, and as its emissivity is higher due to the fact that polar molecules like CO<sub>2</sub> and water are not diluted by the presence of transparent N<sub>2</sub>, it appeared as the right solution.<sup>(3, 8)</sup>

In order to evaluate accurately the expected benefits of the investment, and to anticipate eventual problems caused by the furnace modification, the mathematical model was extended to include a natural gas/oxygen fired zone in the tunnel, with a maximum gas flow rate of 120 Nm<sup>3</sup>/h. The calculation of the maximum DFF productivity was repeated for all products previously limited by the furnace fire power, predicting an increase of 13 % (for an increase of fire-power of 17%). Also, in spite of the high flame temperature of the oxygen/natural gas combustion, computed wall temperatures in the tunnel were lower than 1250 °C, a safe value according to the settings in SIDERAR's furnaces. These conclusions were later verified in the line trials and in the subsequent continuous operation.<sup>(8)</sup>

### ACCURATE STRIP TEMPERATURE MEASUREMENT

An accurate strip temperature measurement is very important in order to obtain consistent processing conditions. As typically occurs, the strip temperature is measured by means of infrared pyrometers, located as described above. The

pyrometers in SIDERAR galvanizing lines are mounted perpendicular to the strip surface, as it is the standard practice in horizontal lines.<sup>(9)</sup> Wedge pyrometry has definite advantages compared to this technique, but it is not easily implemented in a horizontal line, because there are no large rolls inside the furnace where the strip is bent and where the contact between the strip and the roll can be warranted.<sup>(10)</sup>

In spite of being carefully mounted with refrigerated sight tubes in throats partially shielded from the furnaces, the pyrometers reading is influenced by radiation not emitted by the strip. In particular, the location at the exit of the DFF is critical due to the high furnace temperature (up to 1270 °C). As an example, we cite the interesting work undertaken at Dofasco,<sup>(9)</sup> that concludes by comparison with a gold cup pyrometer that a very large diameter refrigerated sight tube (24") can effectively block the furnace radiation.

It is not clear without a detailed analysis what type of instrument is likely to be less affected by extraneous radiation. For instance, the instruments in use at SIDERAR's HDG lines were monochromatic, with wavelengths of 1  $\mu\text{m}$  and 2.3  $\mu\text{m}$ , and it was not clear which one was better. One of the arguments leading to the original selection of the 1  $\mu\text{m}$  instrument was the fact that as strip emissivity is larger at shorter wavelengths, the relative errors introduced by emissivity variations from coil to coil would be minimized. There were, however, large temperature reading variations accompanying changes in material finishing, that could be understood as different influences of the background radiation when the strip surface roughness changed. With the introduction of some two-wavelength pyrometers in the lines, the question of whether to replace or not the monochromatic instruments for this application was set forth.

In order to answer these questions, and understand the role of strip surface characteristics in the suitability of one or the other technique, we developed a model including detailed three-dimensional radiation exchanges, with provision for a detailed model of the optical properties of the strip surface. Full technical details will be reported elsewhere; in the following we discuss the basic ideas behind the model, and some of the results obtained.

The problems involved are readily understood performing a standard three-dimensional enclosure analysis assuming diffuse-gray surfaces. For instance, we could assume the geometry of the DFF exit vestibule represented in Figure 5, where dimensions are in meters. The faces to the left and to the right represent the openings to the DFF and to the radiant tube furnace respectively. The strip is represented in solid color.

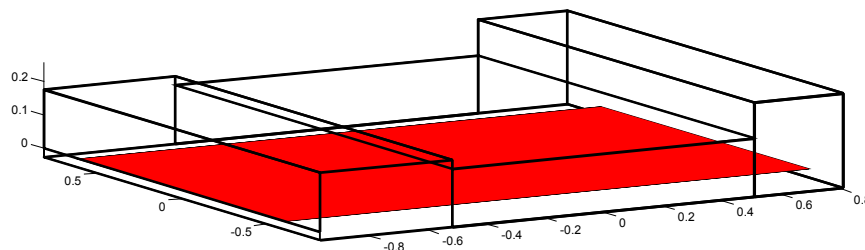


**Figure 5.** Typical vestibule geometry used for radiative exchange computation.

It is quite reasonable to assume that the floor, ceiling and lateral walls are adiabatic (i.e. zero net flux), and to consider the strip and the openings to the furnaces as surfaces with prescribed temperature. A standard enclosure analysis, assuming diffuse gray surfaces with prescribed emissivities, gives equilibrium temperatures for the vestibule walls. Once the whole temperature distribution is known, the radiation issuing from the strip at the sight spot of the pyrometer can be readily computed. Surprisingly, assuming a reasonable strip emissivity of 0.3 and typical temperatures of 1260 °C, 850 °C and 630 °C for the DFF, RTF and strip, respectively, this analysis gives a radiant flux that is more than one order of magnitude larger than the one expected from a black body at the strip temperature. Because the radiating flux measured is comparable to the latter, we conclude that such a model is inadequate.

The main problem is that specular strip reflectivity cannot be neglected if the flux issuing from the strip surface is to be represented accurately. Accordingly, the standard enclosure analysis was extended to include detailed bi-directional reflectivity information. As a trade-off between precision on the one hand and data availability and complexity on the other, we chose to use a simpler approximation, based on what is known as specular-diffuse surfaces: a fixed percentage of the radiating flux impinging on the strip is reflected specularly, while the rest reflects in perfectly diffuse way.<sup>(11-14)</sup> Emission is also diffuse. This kind of approximation is particularly useful in this case because it is fairly simple and there is some experimental data available for cold rolled steel strip.<sup>(15)</sup>

As an example, we show in Figure 6 the inside wall temperature distribution obtained for a 720 mm wide strip, at a temperature of 630 °C, with opening to the DFF at a temperature of 1230 °C and opening to the RTF at 800 °C. This strip is particularly critical from the extraneous radiation viewpoint, because of the high DFF processing temperature (1280 °C) and the little shielding provided by the strip itself. The dark band at the bottom of the opening to the DFF corresponds to the last refrigerated roll in the DFF. Notice also the dark spots in the ceiling and the bottom representing the refrigerated sight tubes of the upper and lower pyrometers. The shielding provided by the strip, which is at a much lower temperature than both the DFF and the RTF, is clearly observed in the temperature of the floor of the vestibule, and less evidently at the ceiling. Predicted typical vestibule internal wall temperatures range from 1000 °C close to the DFF to about 800 °C close to the RTF, clearly lower than DFF temperatures, but significantly hotter than the strip. This means that emission from ceiling regions close to the refrigerated sight tube can have an important contribution to the background radiation reaching the instrument, if the strip surface is not perfectly specular.

In Figure 7 we can observe the predicted pyrometer reading for the same vestibule geometry and strip width, a 1 μm instrument, and corresponding to a 1280 °C DFF, as a function of the assumed strip temperature, for different RTF temperatures. Extremely large errors in the pyrometer reading are thus expected, regardless of the temperature of the RTF, particularly in the low strip temperature range, where the reading is almost insensitive to the true strip temperature. As expected, the error is not as large for high strip temperatures, when the strip emission is significantly higher. One of the practical uses of this kind of curve is that they can be inverted to produce a real temperature indication based on the pyrometer reading, for each strip width and furnaces temperature. This inversion was successfully implemented for the top mounted pyrometer at SIDERAR's CGL #1, which was substantially influenced by background radiation. In particular, the corrected reading was very similar to the reading of the bottom mounted two-wavelength instrument mentioned below.

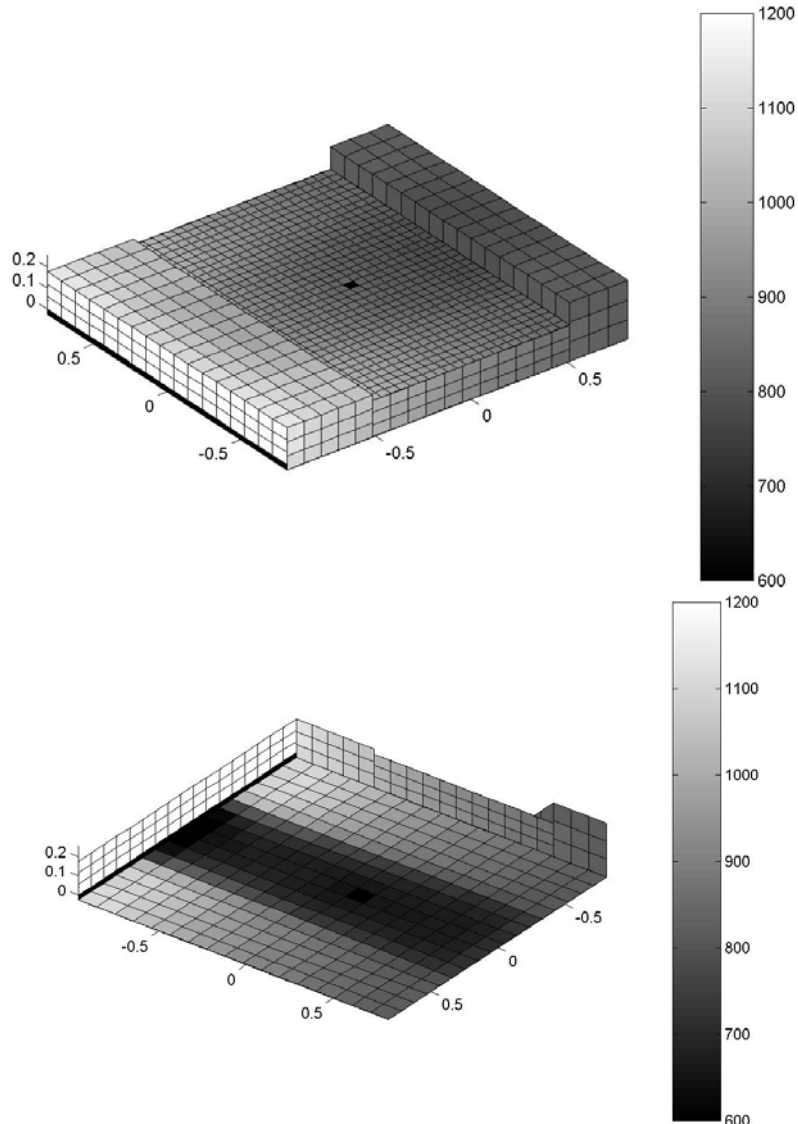


**Figure 6.** Inside wall temperature distribution, for a 720 mm wide strip, at 630 °C, and openings to the DFF and RTF at 1230 °C and 800 °C respectively. The origin of the vertical coordinate is at the pass-line level. a) Top view, b) bottom view.

We wish to stress the fact that this analysis is solidly based on the experimental information available, and yields results that coincide with the experience from the line. It allows to study the influences of the temperatures of the DFF and RTF, the strip width, etc., on the pyrometer reading. The model allowed also to resolve a choice between 1  $\mu\text{m}$  and 2.3  $\mu\text{m}$  pyrometers and to assess the relative merits of the two-wavelength pyrometers for this specific application. The main conclusion can be summarized as follows. At 1  $\mu\text{m}$  the intensity of the emission of the furnace is several orders of magnitude larger than that of the strip. This extreme brightness of the furnace outweighs any advantage obtained from the fact that the strip emissivity is larger than that at 2.3  $\mu\text{m}$ , and in fact the measurement is far more affected by furnace radiation. This conclusion was validated in the line, by changing the temperature of the DFF zone closest to the pyrometer, while maintaining the strip temperature (as recorded by the pyrometer at the exit of the RTF). When this experiment was done with the 1  $\mu\text{m}$  instrument, a large variation in the vestibule

pyrometer reading was observed, while no significant change occurred with the 2.3  $\mu\text{m}$ .

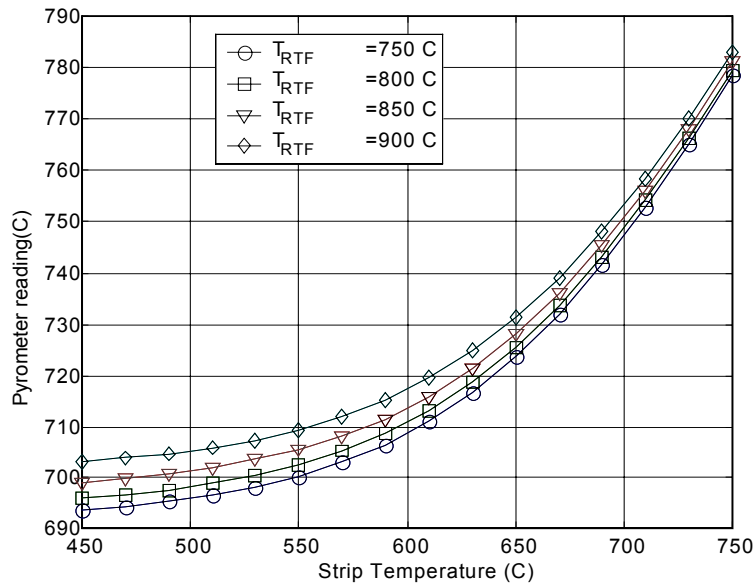


**Figure 7.** Predicted pyrometer reading as a function of the assumed strip temperature, for a 1280 °C DFF, and several RTF temperatures. The pyrometer simulated is a top mounted 1  $\mu\text{m}$  monochromatic instrument, with the vestibule geometry represented in Figure 6.

According to the model, also two-wavelength pyrometers have significant drawbacks when the amount of background radiation is large. This is due to the insignificance of the radiation actually emitted by the strip as compared to the background, and the fact that the e-slope parameter adequate for the strip is typically not adequate to describe the ratio of intensities of the background at the two detection wavelengths. Consequently, at least for the geometry of the exit throat shown, and for the range of furnace temperatures mentioned, the best instrument for the upper mounting location appears to be a monochromatic instrument with relatively long wavelength. As the strip emissivity decreases rapidly with wavelength,<sup>(15,16)</sup> 2.3  $\mu\text{m}$  seems a sensible choice.

There was also a decision regarding if the instrument was to be mounted in the ceiling or in the floor of the exit throat. The main disadvantage of the former is that, as there is need of some 15-20 cm clearance for the threading process, it is not possible to move the sight tube end closer to the strip in order to reduce the amount of reflected radiation. The bottom sight tube, instead, can be placed much closer to the strip because at that location the strip movement is blocked by the rolls. However, both our experience and some reports in the literature<sup>9</sup> indicate that oxide flakes falling down the sight tube of the bottom mounted instrument and accumulating onto the pyrometer lens are a continuous nuisance when using monochromatic pyrometers, because, as the sight path is obscured, the temperature reading diminishes, unless the emissivity setting is continuously (and almost blindly) corrected. As two-wavelength pyrometers are essentially immune to small cold objects placed in the sight path, this deficiency is not so important, and in fact we could use them at the bottom placement with great success.

## ENERGY BALANCE OF THE ZN POT

Strip temperature at the entrance to the molten bath is an important variable both from the coating quality and from the dross formation viewpoints. It was traditionally controlled by a monochromatic pyrometer located at the turn roll hood, which suffered from Zn dust build-up problems. As an almost imperceptible dust coat deposit grows on the pyrometer window, the instrument reading begins to shift towards low temperatures, effectively allowing the strip to enter the molten Zn bath excessively hot. This problem was usually detected only when processing strips with the highest mass flow rate, because the pot heating resistors were off most of the time. In order to have an early warning, and as a cross checking of the pyrometer reading, an energy balance for the Zn pot was developed. As energy inputs we included the heating power of the resistors, the enthalpy flux brought by the strip at the input temperature, and the enthalpy of the Zn ingots at room temperature. As energy outputs, we considered the steel strip and Zn coating enthalpies at the bath temperature, and a single figure to represent the thermal losses (by radiation, convection and conduction). Using the power required to maintain the pot temperature when the line speed is zero and no Zn addition takes place, the losses can be readily estimated. A schematic diagram of the Zn pot is shown in Figure 8.

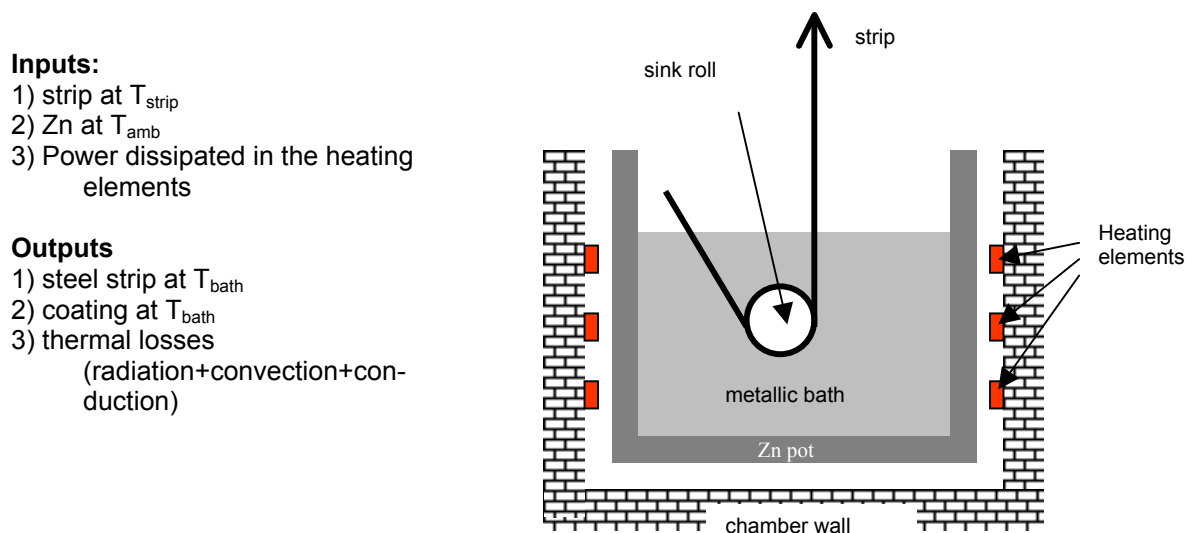


**Figure 8.** Schematic diagram of the Zn pot, indicating inputs and outputs for the energy balance.

As the average energy and mass of the Zn bath are very approximately conserved when considered for relatively long periods, equating the energy inputs to the outputs allows to estimate any term of the energy balance as a function of the rest. In this way, we can obtain an estimate of the heat flux brought by the strip at the entrance to the bath. When the line speed is not zero, this flux can be in turn inverted to yield a strip temperature indication, provided the steel enthalpy as a function of temperature is known.<sup>(5)</sup>

This kind of energy balance was developed and validated for the two SIDERAR's HDG lines, in such a way that each 6-8 hours provides a temperature estimate. If the computed value differs significantly from the measured one, it automatically issues an alarm. As an example of application, Figure 9 shows the evolution of the read and estimated temperatures during a pyrometer failure and its replacement. The strip

temperature set-point was maintained at 475 °C. Notice that despite the fact that the pyrometer reading (represented with circles) is close to the set-point, the predicted strip temperature (squares) is gradually increasing until the instrument is replaced, and then drops to a value close to the pyrometer reading. The solid lines are linear fits, but are only meant to guide the eyes. Observe also the dispersion of the temperature estimation, related to the length of the averaging window. Averaging over longer periods reduces the dispersion, at the expense of yielding coarser time information.

The energy balances also allowed to compare monochromatic and two-wavelength pyrometers, and decide that two-wavelength instruments had a better performance for this specific location in the lines.

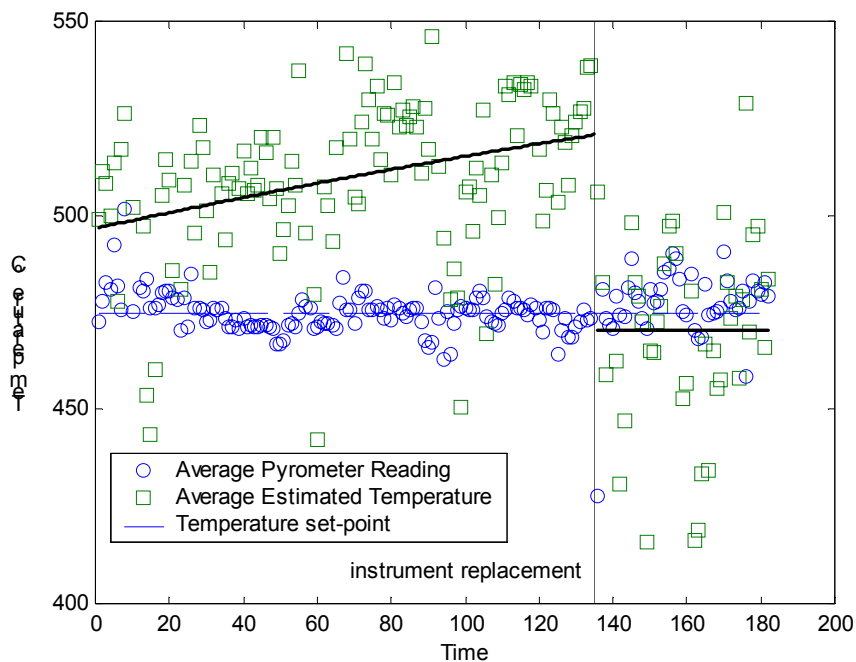


**Figure 9.** Evolution of the estimated temperature during a pyrometer failure and replacement, compared to the average pyrometer reading and strip temperature set-point (475 °C).

## Acknowledgements

We wish to thank Ricardo Alí for their continual support, Pablo Cantarelli who participated in much of the development reported here, Horacio Llano, Walter Pre and Héctor Alvarez for their advice, Alejandro Guerra, Fernando Chalup, Miguel Souza and Andrés Barreiro who contributed to the line trials with their time and dedication, Javier Marek, and the many that contributed to this work over the time.

## REFERENCES

- 1 E. Altschuler, P. Marino, A. Pignotti, D. Migliorino, and A. Jacobsen “Numerical Model of #1 CGL Furnace at SIDERAR”, *Proceedings of the 91<sup>st</sup> Galvanizer’s Conference*, Jackson, MS, USA, October 24-27, 1999.
- 2 E. Altschuler, P. Marino, and A. Pignotti, “Numerical models of reheating gas furnaces in the steel industry”, *Proceedings of the Fourth ISHMT/ASME Heat and*

- Mass Transfer Conference*, Pune, India, January 12-15, 2000, by Tata Mc Graw Hill Publishing House.
- 3 J. M. Rhine, and R. J. Tucker, "*Modelling of Gas-Fired Furnaces and Boilers and Other Industrial Heating Processes*", 1<sup>st</sup> Edition, McGraw-Hill, London, 1991.
  - 4 F. R. Steward, and Y. S. Kocaefe, "Total Emissivity and Absorptivity Models for Carbon Dioxide, Water Vapor and Their Mixtures", *Proceedings of the Eighth International Heat Transfer Conference*, Vol. 2 (1986), pp. 735-740.
  - 5 The British Iron and Steel Research Association, "*Physical Constants of Some Commercial Steels at Elevated Temperatures*", Butterworths Scientific Publications, London, 1953.
  - 6 G. Jankes, M. Stanojevic, M. Karan, M. Kuburovic, M. Adzic. "The use of technical oxygen for combustion processes in industrial furnaces". *Proceedings of the 5<sup>th</sup> European conference on industrial furnaces and boilers*, 11-14 april 2000. Volume I.
  - 7 T. Bougault, S. Desbrosse, P. Slonski, D. Crespo, J.P. Pouchelet, T. Borissoff, G. Le Gouefflec. "Amélioration des performances du four d'une ligne de recuit-décapage de bandes d'acier inoxydable par oxycombustion". *La Revue de Métallurgie-CIT*, Juillet-Aôut 1999, 951-958.
  - 8 G. Cervellini, F. Chalup, J. Etcheverry, D. Migliorino. "Analysis of the incorporation of oxygas combustion technology to a continous galvanizing line". *Proceedings of the 14th Conferencia de Laminación y Primera Conferencia de usos del Acero*, 5-7 november 2002, San Nicolás, Provincia de Buenos Aires, Argentina.
  - 9 J. P. Chaput, J. Gregorio, J. A. Ridge, H. J. Turner, V. W. Tychowsky, "Upgrading and optimization of optical pyrometers at Dofasco's #2 CGL", *Proceedings of the 88<sup>th</sup> Galvanizers's Conference*, Chicago-USA, October 20-23, 1996.
  - 10 J.A. Schulz, J.A. Ridge, R. L. Urquhart. "Application of Wedge pyrometers for strip temperature measurement in a vertical annealing furnace". *Proceedings 95 Galvanizers Conference*, Monterrey, Mexico, 2003.
  - 11 E.M. Sparrow, S. L. Lin. "Radiation heat transfer at a surface having both specular and diffuse reflectance components". *Int. J. Heat Mass Transfer*, Vol. 8, pp. 769-779, 1964.
  - 12 R. P. Bobco. "Radiation Heat transfer in semigray enclosures with specularly and diffusely reflecting surfaces". *J. Heat Transfer*, Feb. 1965, pp. 123-130.
  - 13 A. F. Sarofim, H. C. Hottel. "Radiative Exchange Among non-Lambert surfaces". *J. Heat Transfer*, Feb. 1966, pp. 33-44.
  - 14 R.C. Birkebak, E.M. Sparrow, E.R.G. Eckert, J.M. Ramsey. "Effect of surface roughness on the total hemispherical and specular reflectance of metallic surfaces". *J. Heat Transfer*, May 1964, pp. 193-199.
  - 15 P. Kirby, "Infra-red temperature measurement of steel strip in the hot dip galvanizing process". 1990, *Internal Report*, Land Infrared Division.
  - 16 R. Siegel, J. Howell, "Thermal Radiation Heat Transfer", 3<sup>rd</sup> Edition, Taylor & Francis, Washington, 1992.